JOURNAL OF MATERIALS SCIENCE 29 (1994) 5135–5140

Pull-out of a ductile fibre from a brittle matrix

PART II *A simplified model*

CHUN-HWAY HSUEH
Metals and Ceramics Division, Oak Ridge National Laboratory, Oak Ridge, Tennessee 37831, USA

The pull-out of a ductile fibre from a brittle matrix was analysed in Part I [1] using a shear-lag model. However, the analysis is formidable due to the consideration of Poisson's effect along the sliding length. This consideration is essential when the debonded fibre–matrix interface is subjected to Coulomb friction during fibre pull-out. To simplify the analysis, Poisson's effect is treated in an average sense in the present study, whereas it was treated pointwise in Part I. The present simplified solutions are in excellent agreement with the previous more rigorous and more complex solutions. The simplified model thus provides adequate solutions for the pull-out of a ductile fibre from a brittle matrix, and can be readily used for further applications.

1. Introduction

Interfacial debonding, fibre yielding and necking occur during pull-out of a ductile fibre from a brittle matrix. When the debonded interface is subjected to Coulomb friction, which is proportional to the radial compression at the interface, consideration of Poisson's effect is essential. During pull-out, the fibre is subjected to axial tension, and radial tension is induced at the interface due to Poisson's effect, which, in turn, modifies the resultant interfacial radial stress. In the presence of both Poisson's effect and plasticity of the fibre, the stress analysis for the pull-out problem was made in Part I [1] using a shear-lag model; however, the analysis is formidable. When the pull-out analysis is incorporated to solve other problems, the complexity in the analysis will be compounded. For example, the analysis of the toughening effect due to fibre bridging in a ceramic-matrix composite requires a double integral of the stress–displacement relation of the pull-out fibres along the crack surface [2]. Hence, to facilitate the application of the pull-out analysis, a simplified analysis is imperative.

The complexity of the pull-out analysis arises mainly from Poisson's effect, which results in a non-uniform interfacial shear stress along the sliding length. Hence, to simplify the analysis, Poisson's effect along the sliding length is not considered pointwise but is considered in an average sense in the present study. This averaging technique has been successfully adopted to analyse pull-out of a brittle fibre from a brittle matrix [3]. To justify the applicability of the averaging technique to pull-out of a ductile fibre from a brittle matrix, the simplified solutions obtained in the present study are compared to the previous complex solutions [1]. Excellent agreement is obtained in this comparison. Also, due to the complexity of the analyses, the previous model [1] is limited to the conditions that the interface has a finite bond strength and the fibre undergoes linear strain hardening. Using the present simplified model, the solutions for an unbonded interface and power-law strain hardening of the fibre are also obtained.

2. A simplified model

The geometry considered in Part I for the fibre-pull-out problem is shown in Fig. 1. A ductile fibre with

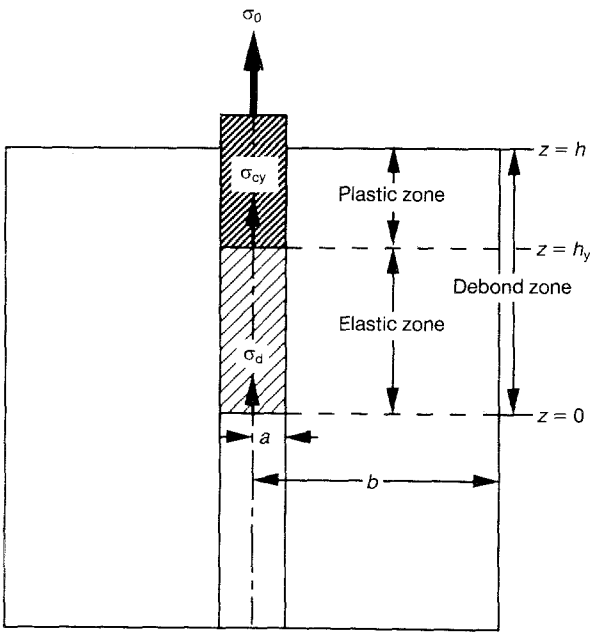

Figure 1 Schematic showing the simplified model used in analysing pull-out of a ductile fibre from a brittle matrix. The debond length is h, which consists of an elastic and a plastic zone length (h_y and $h - h_y$). The axial stress in the fibre is σ_{cy} at $z = h_y$, and is σ_d at $z = 0$.

0022–2461

a radius, a, is located at the centre of a coaxial cylindrical shell of a brittle matrix with an outer radius, b. A stress, σ_0, is applied to the fibre in the axial direction, z. When σ_0 exceeds the interfacial bond strength σ_d, interfacial debonding and sliding occur within a length h, such that the axial stress in the fibre is in equilibrium with σ_d at the end of the sliding zone. It was shown in Part I that the yield stress of a constrained (that is, embedded) fibre, σ_{cy}, is different from that of an unconstrained fibre, σ_y. When σ_0 reaches σ_{cy}, yielding occurs, and both the plastic zone length $(h - h_y)$ and the debond length, h, increase with increasing σ_0. At the end of the plastic zone, the axial stress in the fibre (that is, σ_f at $z = h_y$) changes with the plastic-zone length due to the varying degree of the constraint which, in turn, results in a change in the elastic-zone length, h_y, after yielding [1]. However, these changes in σ_f at $z = h_y$ and in h_y are negligible [1]. Hence, after yielding, both σ_f at $z = h_y$ and h_y are assumed to be constants in the present model. Furthermore, $\sigma_f = \sigma_{cy}$ at $z = h_y$ (which is the boundary condition at the end of the plastic zone).

Poisson's effect along the sliding length is treated in an average sense in the present model. When the fibre remains elastic during the pull-out process, the solutions are as obtained previously [3]. However, when the fibre becomes ductile, the background of the analyses in [3] is required for the present study. Hence, without yielding of the fibre, the analyses [3] are summarized in Section 2.1. When yielding occurs, the solutions can be obtained by modifying the analyses in Section 2.1 and they are presented in Section 2.2.

2.1. Elastic solutions (for $\sigma_0 \leq \sigma_{cy}$)

For a frictional interface, the axial stresses in the fibre and the matrix, σ_f and σ_m, vary slowly over distances comparable to the fibre radius. In this case, the characteristics of stresses in any section transverse to the axial direction can be approximated by a Lamé problem, and both σ_f and σ_m can be approximated as being independent of the radial coordinate [4, 5]. The condition that the fibre and the matrix remain in contact during frictional sliding requires continuity of the radial displacement (or the tangential strain) at the interface. Considering the Lamé problem and satisfying the continuity condition, the interfacial radial stress, σ_p, induced due to Poisson's effect is [3–7]

$$\sigma_p = \frac{1}{D}\left[\left(\frac{\nu_f E_m}{E_f} + \frac{a^2\nu_m}{b^2 - a^2}\right)\sigma_f - \frac{a^2\nu_m\sigma_0}{b^2 - a^2}\right] \quad (1)$$

where E and ν are Young's modulus and Poisson's ratio, the subscripts f and m denote the fibre and the matrix, respectively, and D is given by

$$D = \frac{b^2 + a^2}{b^2 - a^2} + \nu_m + \frac{(1 - \nu_f)E_m}{E_f} \quad (2)$$

The axial stress in the fibre, σ_f, varies along the sliding length due to the stress transfer. Hence, when Poisson's effect is considered pointwise, σ_p (Equation 1) varies along the sliding length. However, when Poisson's effect is treated in an average sense, only the average values along the sliding length of both σ_p and the interfacial frictional stress, τ_i, (that is, $\bar{\sigma}_p$ and $\bar{\tau}_i$) are considered. With a uniform $\bar{\tau}_i$, σ_f varies linearly from σ_0 at the loaded surface to σ_d at the end of the sliding zone, such that its average value along the sliding length is

$$\bar{\sigma}_f = \frac{\sigma_0 + \sigma_d}{2} \quad (3)$$

Substituting Equation 3 into Equation 1, $\bar{\sigma}_p$ becomes

$$\bar{\sigma}_p = \frac{1}{2D}\left[\left(\frac{\nu_f E_m}{E_f} - \frac{a^2\nu_m}{b^2 - a^2}\right)\sigma_0 + \left(\frac{\nu_f E_m}{E_f} + \frac{a^2\nu_m}{b^2 - a^2}\right)\sigma_d\right] \quad (4)$$

and the corresponding $\bar{\tau}_i$ is

$$\bar{\tau}_i = \mu(\sigma_c + \bar{\sigma}_p) \quad (5)$$

where μ is the coefficient of friction, and σ_c is the interfacial residual clamping stress (negative). The sign of the shear stress signifies the direction of shear, and $\bar{\tau}_i$ is negative due to the co-ordinate system used in the present study.

Adopting the average interfacial frictional stress, the sliding-zone length, h, is

$$h = \frac{a(\sigma_d - \sigma_0)}{2\bar{\tau}_i} \quad (6)$$

Substitution of Equations 4 and 5 into Equation 6 yields the applied-stress–sliding-zone-length relation, such that, for $\sigma_0 \leq \sigma_{cy}$,

$$\sigma_0 = \left\{\left[1 - \frac{h\mu}{aD}\left(\frac{\nu_f E_m}{E_f} + \frac{a^2\nu_m}{b^2 - a^2}\right)\right]\sigma_d - \frac{2h\mu\sigma_c}{a}\right\} \times \left[1 + \frac{h\mu}{aD}\left(\frac{\nu_f E_m}{E_f} - \frac{a^2\nu_m}{b^2 - a^2}\right)\right]^{-1} \quad (7)$$

The axial displacement of the fibre at the loaded end, w, obtained from integration of the axial strain along the sliding length is

$$w = \frac{h(\bar{\sigma}_f - 2\nu_f\bar{\sigma}_p)}{E_f} \quad (8a)$$

However, $\bar{\sigma}_f \gg 2\nu_f\bar{\sigma}_p$, and w can be approximated by

$$w = \frac{h(\sigma_0 + \sigma_d)}{2E_f} \quad (8b)$$

2.2. Elastic/plastic solutions (for $\sigma_0 \geq \sigma_{cy}$)

When σ_0 reaches σ_{cy}, yielding initiates at the loaded surface. Using the Von Mises yield criterion [8], the yield stress of the constrained fibre, σ_{cy}, can be related to the yield stress of the unconstrained fibre, σ_y, by [1]

$$\sigma_{cy} = \sigma_c + \sigma_p + \sigma_y \quad (9)$$

Substituting Equation 1 into Equation 9, and letting $\sigma_0 = \sigma_{cy}$ for initiation of yielding at the loaded surface (where $\sigma_f = \sigma_0$), σ_{cy} can be solved such that

$$\sigma_{cy} = \frac{\sigma_c + \sigma_y}{1 - \frac{\nu_f E_m}{DE_f}} \tag{10}$$

Hence, when the fibre is under a strong residual clamping stress, the tensile yield stress of a constrained fibre can be smaller than that of an unconstrained fibre. However, in the absence of σ_c, σ_{cy} becomes greater than σ_y for the fibre pull-out test.

After yielding, the debond length consists of an elastic- and a plastic zone length. The solutions for the elastic zone (that is, for $h_y \geq z \geq 0$ in Fig. 1) can be obtained from Section 2.1. by substituting σ_0 with σ_{cy} in the solutions, and the fibre displacement at $z = h_y$ (that is, the fibre displacement in the elastic zone, w_e) is

$$w_e = \frac{h_y(\sigma_{cy} + \sigma_d)}{2E_f} \tag{11}$$

The solutions for the plastic zone (that is, $h \geq z \geq h_y$ in Fig. 1) can be obtained by modifying the analyses in Section 2.1, as follows.

If the fibre exhibits linear strain hardening, the plastic strains in the fibre are [1, 9]

$$\varepsilon_z^p = \frac{\sigma_f - \sigma_c - \sigma_p - \sigma_y}{H} \tag{12a}$$

$$\varepsilon_r^p = \varepsilon_\theta^p = -\frac{\sigma_f - \sigma_c - \sigma_p - \sigma_y}{2H} \tag{12b}$$

where H is the slope of the strain-hardening curve. In the presence of plasticity of the fibre, the plastic-strain component should be included in the condition of continuity of the tangential strain at the interface, such that

$$\frac{(1 - \nu_f)\sigma_p - \nu_f\sigma_f}{E_f} - \frac{\sigma_f - \sigma_c - \sigma_p - \sigma_y}{2H} = \frac{-\left(\frac{b^2 + a^2}{b^2 - a^2} + \nu_m\right)\sigma_p - \nu_m\sigma_m}{E_m} \tag{13}$$

It should be noted that whereas the radial dependence of the axial stress in the matrix was considered in Part I (see Equation 9 in Part I), this radial dependence is not considered in the present model (see Equation 13).

Using the above continuity condition, letting $\sigma_f = \sigma_{cy}$ at the end of the plastic zone (that is, at $z = h_y$), and repeating the calculation procedures in Section 2.1, the relation between the applied stress and the plastic-zone length, $h - h_y$, is

$$\sigma_0 = \left(\left\{1 - \frac{(h - h_y)\mu}{a\left(D + \frac{E_m}{2H}\right)}\left[\frac{\nu_f E_m}{E_f} + \frac{a^2\nu_m}{b^2 - a^2} + \frac{E_m}{H}\left(\frac{\nu_f E_m}{DE_f} - \frac{1}{2}\right)\right]\right\}\sigma_{cy} - \frac{2(h - h_y)\mu\sigma_c}{a}\right) \times \left[1 + \frac{(h - h_y)\mu}{a(D + E_m/2H)} \times \left(\frac{\nu_f E_m}{E_f} - \frac{a^2\nu_m}{b^2 - a^2} + \frac{E_m}{2H}\right)\right] \tag{14}$$

The corresponding average interfacial frictional stress, $\bar{\tau}_i$, and fibre displacement (due to the plastic zone), w_p, are

$$\bar{\tau}_i = \mu\left\{\sigma_c + \frac{\left(\frac{\nu_f E_m}{E_f} - \frac{a^2\nu_m}{b^2 - a^2} + \frac{E_m}{2H}\right)\sigma_0 + \left[\frac{\nu_f E_m}{E_f} + \frac{a^2\nu_m}{b^2 - a^2} + \frac{E_m}{H}\left(\frac{\nu_f E_m}{DE_f} - \frac{1}{2}\right)\right]\sigma_{cy}}{2D + E_m/H}\right\} \tag{15a}$$

$$w_p = \left[\left(\frac{1}{E_f} + \frac{1}{H}\right)\frac{\sigma_0 + \sigma_{cy}}{2} - \frac{1}{H}\left(\frac{\bar{\tau}_i}{\mu} + \sigma_y\right)\right](h - h_y) \tag{15b}$$

The resultant fibre displacement, w, is the summation of the components due to displacements in both the elastic zone and the plastic zone, such that

$$w = w_e + w_p \tag{16}$$

It should be noted that the induced interfacial radial tension, σ_p, due to Poisson's effect can compensate the residual clamping stress, σ_c, and result in a frictionless interface [4, 5, 10, 11]. This would start at the loaded surface, where Poisson's effect is the greatest, and it is not considered in the averaging technique. Hence, the present analysis for pull-out is subjected to the condition that the pull-out stress is limited by a critical value such that [5, 10, 11]

$$\sigma_0 \leq -\frac{DE_f\sigma_c}{\nu_f E_m} \tag{17a}$$

when the fibre remains elastic (that is, $\sigma_0 < \sigma_{cy}$), and

$$\sigma_0 \leq \frac{-D\sigma_c + E_m\sigma_y/2H}{\nu_f E_m/E_f + E_m/2H} \tag{17b}$$

when the fibre yields (that is, $\sigma_0 > \sigma_{cy}$).

3. Unbonded interfaces

For a bonded interface, the axial stress in the fibre is in equilibrium with the bond strength, σ_d, at the end of the debond zone. For an unbonded interface, redefinition of σ_d at the end of the debond (elastic) zone is required. However, the solutions for the plastic zone are independent of the condition at the end of the

elastic zone. When the interface is unbonded, upon loading the fibre, interfacial sliding begins at the loaded surface and extends some depth beneath the surface. The end of the sliding zone is characterized by the condition that the axial strain in the fibre is equal to that in the matrix, such that

$$\frac{\sigma_f - 2\nu_f\sigma_p}{E_f} = \frac{\sigma_m + \dfrac{2a^2\nu_m\sigma_p}{b^2 - a^2}}{E_m} \quad (\text{at } z = 0) \tag{18}$$

Replacing the boundary condition that $\sigma_f = \sigma_d$ at $z = 0$ for a bonded interface by Equation 18 for an unbonded interface, and repeating the calculation procedures in Section 2, the stress–elastic-zone-length relation for an unbonded interface is

$$\sigma_0 = \frac{-2h\mu\sigma_c/a}{1 + \dfrac{h\mu}{aD}\left(\dfrac{\nu_f E_m}{E_f} - \dfrac{a^2\nu_m}{b^2 - a^2}\right) - \gamma\left[1 - \dfrac{h\mu}{aD}\left(\dfrac{\nu_f E_m}{E_f} + \dfrac{a^2\nu_m}{b^2 - a^2}\right)\right]} \tag{19}$$

where

$$\gamma = \left[\frac{a^2}{b^2 - a^2} - \frac{2a^2\nu_m}{(b^2 - a^2)D}\left(\frac{\nu_f E_m}{E_f} + \frac{a^2\nu_m}{b^2 - a^2}\right)\right] \times \left[\frac{a^2}{b^2 - a^2} + \frac{E_m}{E_f} - \frac{2}{D}\left(\frac{\nu_f E_m}{E_f} + \frac{a^2\nu_m}{b^2 - a^2}\right)^2\right]^{-1} \tag{20}$$

The solutions for $\bar{\sigma}_p$, $\bar{\tau}_i$, h, and w can be obtained from Equations 4–6 and Equation 8 by replacing σ_d with $\gamma\sigma_0$.

4. Power-law strain hardening

The solutions for the elastic zone are independent of the strain-hardening behaviour of the fibre. For power-law strain hardening, the plastic strains can be described by the Ludwik equation [8] such that

$$\varepsilon_z^p = \left(\frac{\sigma_f - \sigma_c - \sigma_p - \sigma_y}{K}\right)^{1/n} \tag{21a}$$

$$\varepsilon_r^p = \varepsilon_\theta^p = -\frac{1}{2}\left(\frac{\sigma_f - \sigma_c - \sigma_p - \sigma_y}{K}\right)^{1/n} \tag{21b}$$

where n is the strain-hardening exponent, and K is the strength coefficient.

Substituting the plastic-strain component in Equation 13 for linear strain hardening by Equation 21b for power-law strain hardening, and repeating the calculation procedures in Section 2, the stress–plastic-zone-length relation becomes

$$\sigma_0 = \left\{\left[1 - \frac{(h - h_y)\mu}{aD}\left(\frac{\nu_f E_m}{E_f} + \frac{a^2\nu_m}{b^2 - a^2}\right)\right]\sigma_{cy} - \frac{2(h - h_y)\mu\sigma_c}{a} - \frac{(h - h_y)\mu E_m}{aD} \times \left[\frac{\sigma_0 + \sigma_{cy} - 2(\sigma_c + \bar{\sigma}_p + \sigma_y)}{2K}\right]^{1/n}\right\} \times \left[1 + \frac{(h - h_y)\mu}{aD}\left(\frac{\nu_f E_m}{E_f} - \frac{a^2\nu_m}{b^2 - a^2}\right)\right] \tag{22}$$

The corresponding values of $\bar{\sigma}_p$, and w_p are

$$\bar{\sigma}_p = \left(\frac{\nu_f E_m}{E_f} - \frac{a^2\nu_m}{b^2 - a^2}\right)\frac{\sigma_0}{2D} + \left(\frac{\nu_f E_m}{E_f} + \frac{a^2\nu_m}{b^2 - a^2}\right)\frac{\sigma_{cy}}{2D} + \frac{E_m}{2D}\left[\frac{\sigma_0 + \sigma_{cy} - 2(\sigma_c + \bar{\sigma}_p + \sigma_y)}{2K}\right]^{1/n} \tag{23}$$

$$w_p = \left\{\frac{\sigma_0 + \sigma_{cy}}{2E_f} + \left[\frac{\sigma_0 + \sigma_{cy} - 2(\sigma_c + \bar{\sigma}_p + \sigma_y)}{2K}\right]^{1/n}\right\} \times (h - h_y) \tag{24}$$

It should be noted that the right-hand side of Equation 22 contains σ_0 and $\bar{\sigma}_p$, and numerical iterations are required to obtain the relation between σ_0 and $h - h_y$. The iteration procedure commences with the solutions for a zero plastic-zone length such that

$$\sigma_0 = \sigma_{cy} \quad (h - h_y \to 0) \tag{25a}$$

$$\bar{\sigma}_p = \frac{\nu_f E_m \sigma_{cy}}{DE_f} \quad (h - h_y \to 0) \tag{25b}$$

as the trial solutions. Then for a small increment of the plastic-zone length, the trial solutions of σ_0 and $\bar{\sigma}_p$ are substituted into the right-hand sides of Equations 22 and 23 to calculate a new pair of σ_0 and $\bar{\sigma}_p$, which are then used as the trial solutions. This process is iterated until constant values of σ_0 and $\bar{\sigma}_p$ are approached, which are the solutions. These solutions are then used as the trial solutions for the next small increment of the plastic-zone length. The processes are repeated until the desired plastic-zone length is reached.

5. Results

First, the simplified solutions obtained in the present study are compared with the previous rigorous solutions for the linear-strain-hardening case. Then, the solutions for the unbonded interface are presented. Finally, an example of the solutions for the power-law strain-hardening case is given.

5.1. Comparison (for linear strain hardening)

The material properties used in Part I (that is, for W-3Re fibre-reinforced TiTaAl composites:

$E_f = 350$ GPa, $E_m = 215$ GPa, $\nu_f = 0.28$, $\nu_m = 0.238$, $\sigma_c = -823.5$ MPa, $\sigma_y = 1.9$ GPa, $H = 250$ GPa, $\mu = 0.2$, $a = 37.5$ μm, $b/a = 10$ and $\sigma_d = 80$ MPa) are adopted for the analysis. Using Equation 10, the yield stress of the constrained fibre is ~ 1.2 GPa, which is in excellent agreement with the result derived in Part I. Both the debond length and the plastic-zone length, as functions of the applied stress, are shown in Fig. 2. Excellent agreement between the previous [1] and the present solutions were obtained.

The distributions of the axial stress in the fibre and the interfacial shear stress along the debond length are shown in Fig. 3 for $\sigma_0 = 2.038$ GPa. Excellent agreement between the previous and the present analyses were obtained for σ_f. Whereas the previous solutions offered the shear-stress distribution along the sliding length, the present solutions can only give the average interfacial shear stresses in the plastic and the elastic zones. However, these average interfacial shear stresses are sufficient to evaluate the frictional resistance along the sliding length.

For the shear-lag model, the solutions for the sliding displacement of the fibre at the loaded surface are given in the Appendix. The stress–sliding-displacement relations are shown in Fig. 4, and excellent agreement between the shear-lag model and the present simplified model was obtained.

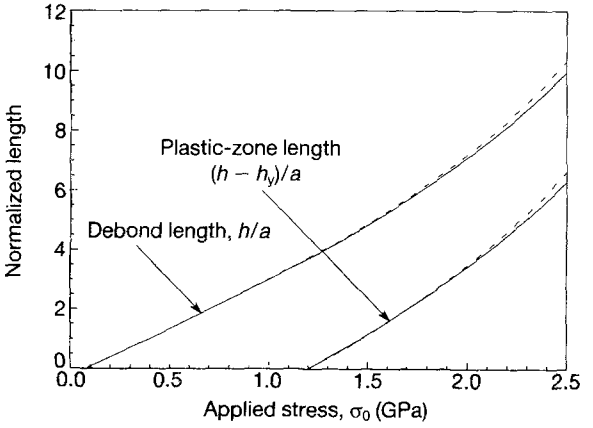

Figure 2 The debond length, h, and the plastic-zone length, $h - h_y$, as functions of the applied stress. (——) simplified model, and (– – –) shear-lag model.

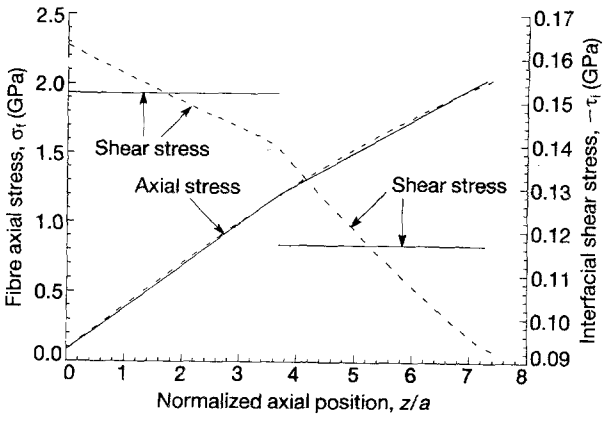

Figure 3 The axial stress in the fibre, σ_f, and the interfacial shear stress, $-\tau_i$, as functions of the normalized axial position, z/a, for $\sigma_0 = 2.038$ GPa: (——) simplified model, and (– – –) shear-lag model.

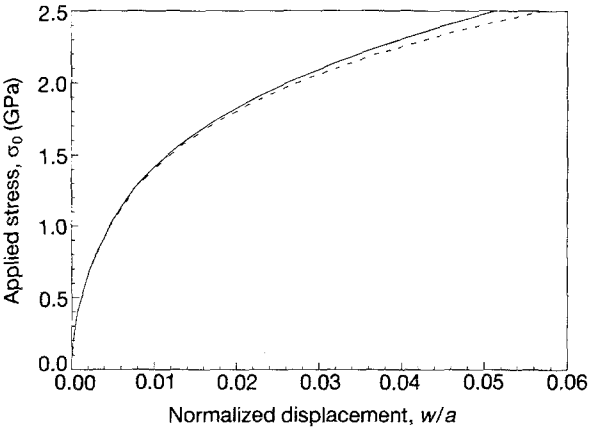

Figure 4 The stress–displacement relation: (——) simplified model, and (– – –) shear-lag model.

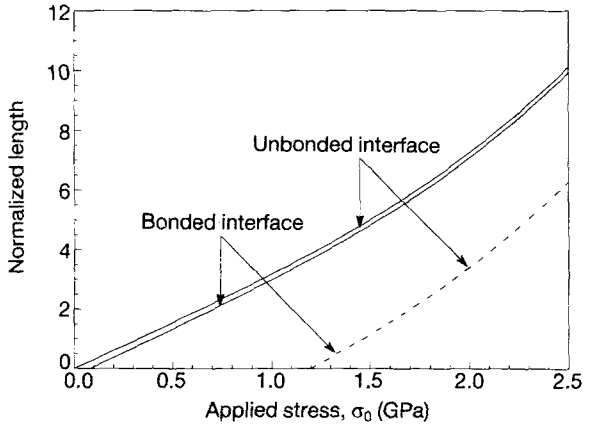

Figure 5 The sliding length, h, and the plastic-zone length, $h - h_y$, as functions of the applied stress for a bonded interface ($\sigma_d = 80$ MPa) and an unbonded interface.

5.2. Unbonded interfaces

When the interface is unbonded, σ_f at the end of sliding zone is not a constant; it is proportional to the applied stress (that is, $\sigma_d = \gamma\sigma_0$). Using the material properties in Section 5.1, but replacing $\sigma_d = 80$ MPa by the condition for an unbonded interface (that is, by Equation 18), the calculated sliding length and the plastic-zone length are shown in Fig. 5. The solutions for a bonded interface, $\sigma_d = 80$ MPa, are also shown. Both the bonded and the unbonded interfaces have the same plastic-zone length. Compared to the bonded interface, the unbonded interface has a greater sliding length.

5.3. Power-law strain hardening

The numerical solutions presented in Section 4 can be confirmed by using $n = 1$ and $K = H$. In this case, the power-law strain hardening becomes linear strain hardening, and the calculated results from numerical iterations should be identical to those from the analytical solutions presented in Section 2. Using $K = 250$ GPa, the calculated debond length and the plastic-zone length are shown in Fig. 6 for different values of n. The plastic strain decreases with decreasing n. While the elastic-zone length is not influenced by the power-law strain hardening, the plastic-zone length (and hence the debond length) decreases with decreasing n.

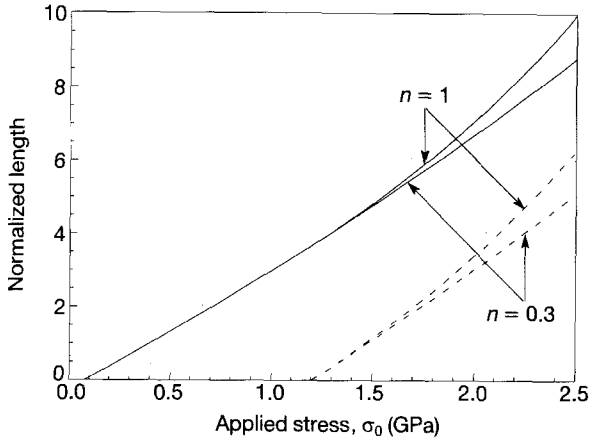

Figure 6 The debond length, h, and the plastic-zone length, $h - h_y$, as functions of the applied stress for linear strain hardening ($n = 1$) and power-law strain hardening ($n = 0.3$). (——) debond length, h/a, (– – –) plastic zone length $(h - h_y)/a$.

6. Conclusion

During fibre pull-out, the stress is transferred from the fibre to the matrix through the interfacial shear stress. An interfacial radial stress is induced due to axial loading on the fibre and the constraint at the interface (that is, Poisson's effect). When the interface is bonded, the interfacial shear stress is insensitive to the change of the interfacial radial stress induced by Poisson's effect. However, when the interface is debonded and is subjected to Coulomb friction, Poisson's effect plays an important role on the interfacial shear stress. Considering Poisson's effect along the sliding length, pointwise, stress analyses for pull-out of a ductile fibre from a brittle matrix were made in Part I using a shear-lag model. However, the solutions are formidable, which, in turn, results in an obstacle to their further application. Also, the analyses in Part I are limited to the conditions that the interface has a constant bond strength and the fibre is linear strain hardened.

In the present study, Poisson's effect along the sliding length was treated in an average sense, and both the stress analysis and the solutions for pull-out of a ductile fibre from a brittle matrix are greatly simplified. The simplified solutions obtained in the present study were compared to the previous complicated, rigorous solutions, and excellent agreement was obtained. The simplified model thus provides adequate solutions for pull-out of a ductile fibre from a brittle matrix. This averaging technique was then applied to the case of an unbonded interface and to power-law strain hardening of the fibre.

Appendix

Fibre displacement from the shear-lag model [1]. The axial displacement of the fibre can be obtained by integrating the axial strain along the debond length. The displacements due to the elastic zone and the plastic zone, w_e and w_p, are:

$$w_e = \frac{1}{E_f}\left\{\frac{A_3}{A_2}\left[z - \frac{\exp(m_2 z) - 1}{m_2}\right] + B\left[\frac{\exp(m_1 z) - 1}{m_1} - \frac{\exp(m_2 z) - 1}{m_2}\right] + \frac{[\exp(m_2 z) - 1]\sigma_d}{m_2}\right\} \quad \text{(A1)}$$

$$w_p = \left(\frac{1}{E_f} + \frac{1}{H}\right) \times \left\{\frac{B_3}{B_2}\left[z - h_y - \frac{\exp(n_2 z) - \exp(n_2 h_y)}{n_2 \exp(n_2 h)}\right] + C\left[\frac{\exp(n_1 z) - \exp(n_1 h_y)}{n_1} - \frac{\exp[(n_1 - n_2)h][\exp(n_2 z) - \exp(n_2 h_y)]}{n_2}\right] + \frac{[\exp(n_2 z) - \exp(n_2 h_y)]\sigma_0}{n_2 \exp(n_2 h)}\right\} + \frac{a}{2\mu H}\left\{\frac{B_3}{B_2}\left[\frac{\exp(n_2 h_y) - \exp(n_2 z)}{\exp(n_2 h)}\right] + C[\exp(n_1 z) - \exp(n_1 h_y) - \exp[(n_1 - n_2)h] \times \{\exp(n_2 z) - \exp(n_2 h_y)\}] + \left[\frac{\exp(n_2 z) - \exp(n_2 h_y)}{\exp(n_2 h)}\right]\sigma_0\right\} - \frac{(z - h_y)\sigma_y}{H} \quad \text{(A2)}$$

The parameters in Equations A1 and A2 are defined in [1].

Acknowledgements

The author thanks Drs P. F. Becher, J. M. Schneibel and E. Lara-Curzio for reviewing the manuscript. Research sponsored by the US Department of Energy, Division of Materials Sciences, under contract DE-AC05-84OR21400 with Martin Marietta Energy Systems, Inc.

References

1. C. H. HSUEH, *J. Mater. Sci.*, submitted.
2. I. N. SNEDDON and M. LOWENGRUB, in "Crack problems in the classical theory of elasticity" (John Wiley, New York, 1969) p. 27.
3. C. H. HSUEH, *Mater. Sci. Engng. A* **161** (1973) 41.
4. J. W. HUTCHINSON and H. M. JENSEN, *Mech. Mater.* **9** (1990) 139.
5. Y. C. GAO, Y. W. MAI and B. COTTERELL, *J. Appl. Math. and Phys. (ZAMP)* **39** (1988) 550.
6. L. S. SIGL and A. G. EVANS, *Mech. Mater.* **8** (1989) 1.
7. W. B. TSAI and T. MURA, *Comp. Engng.* **3** (1993) 101.
8. R. HILL, "The Mathematical theory of plasticity" (Clarendon Press, Oxford, 1950).
9. C. H. HSUEH and A. G. EVANS, *J. Amer. Ceram. Soc.* **68** (1985) 120.
10. C. H. HSUEH, *Mater. Sci. Engng. A* **149** (1991) 11.
11. H. TSUDA, M. ENOKI and T. KISHI, *J. Ceram. Soc. Jpn* **100** (1992) 530.

Received 30 March
and accepted 8 July 1993